Directional Laser Emission from a Wavelength-Scale Chaotic Microcavity

Q. H. Song,[1] L. Ge,[1] A. D. Stone,[1] H. Cao,[1] J. Wiersig,[2] J.-B. Shim,[2] J. Unterhinninghofen,[2] W. Fang,[3] and G. S. Solomon[3]

[1]*Department of Applied Physics, Yale University, New Haven, Connecticut 06520-8482, USA*

[2]*Institut für Theoretische Physik, Universität Magdeburg, Postfach 4120, D-39016 Magdeburg, Germany*

[3]*Joint Quantum Institute, NIST and University of Maryland, Gaithersburg, Maryland 20899, USA*

(Received 28 February 2010; revised manuscript received 21 July 2010; published 31 August 2010)

We demonstrate directional output from a deformed disk laser of dimensions comparable to the emission wavelength. Unlike larger deformed cavity lasers, which exhibit universal output directionality determined by chaotic ray dynamics, the far-field patterns differ between lasing modes. The directional emission results from weak coupling of isotropic high-quality modes to anisotropic low-quality modes, combined with chiral symmetry breaking of clockwise and counterclockwise propagating waves. This mechanism makes it possible to control the output properties of wavelength-scale lasers.

DOI: 10.1103/PhysRevLett.105.103902 PACS numbers: 42.55.Sa, 05.45.Mt, 42.25.−p, 42.60.Da

Confinement and manipulation of light in optical microcavities has been a subject of intense fundamental and applied research for more than a decade [1]. One prominent example is the microdisk whose high quality factor ($Q = \omega/\Delta\omega$, where ω is the resonance frequency and $\Delta\omega$ the linewidth) and in-plane output make it a promising candidate for on-chip optoelectronic devices [1]. Recently, there has been a strong pursuit of nanoscale coherent light sources, important to nanophotonics and high density photonic circuits [2,3]. A key issue is the efficient generation and collection of the light emitted from such small cavities. Since circular disks have isotropic emission patterns, some method must be employed to break this symmetry, e.g., by positioning of a nearby tapered fiber; however, standard fiber coupling is significantly limited by the large size of fiber, precise position control, and optical force of resonant modes [1].

Another approach is to deform the cavity from circular symmetry in a manner which generates intrinsically directional emission [4]. The typical shapes generate chaotic ray dynamics in most of the phase space. The directional emission pattern from such asymmetric resonant cavities (ARCs) was predictable from knowledge of the phase space dynamics and, in particular, from the geometry of the unstable manifolds of short unstable periodic orbits (UPOs) [5]. Directional emission based on this approach has been demonstrated experimentally in a number of systems [5–10]. Recently a special ARC based on a dipolar deformation of the circle (known as the limaçon cavity) was shown [11] to have unidirectional emission combined with relatively high-Q factor. Several experiments confirmed this prediction [12] for cavities significantly larger than the wavelength of the emitted light; wavelength-scale ARC lasers have not been studied.

The model explaining and predicting directional emission [5] is expected to break down as the wavelength approaches the cavity size and wave transport differs substantially from ray transport. It is therefore interesting to see if smoothly deformed *wavelength-scale* cavities can still achieve simultaneously unidirectional emission and high-Q factor. In this Letter, we demonstrate unidirectional emission from wavelength-scale lasers. which is not explicable by the ray model, and we show that it arises from the coupling of relatively isotropic high-Q mode (HQM) to more directional low-Q mode (LQM).

We fabricated GaAs microdisk lasers with embedded InAs quantum dots as the gain media. Our sample fabrication procedure and lasing experimental setup are similar to those in Ref. [12]. The inset of Fig. 1(a) is a top-view scanning electron microscope (SEM) image of a GaAs ARC inspired by the limaçon, which can be fitted in polar coordinates by $\rho(\theta) = R(1 + \epsilon\cos\theta)(1 - \epsilon_1\cos 2\theta) + d$, where $R = 890$ nm, $\epsilon = 0.28$, $\epsilon_1 = 0.06$, and $d = 60$ nm.

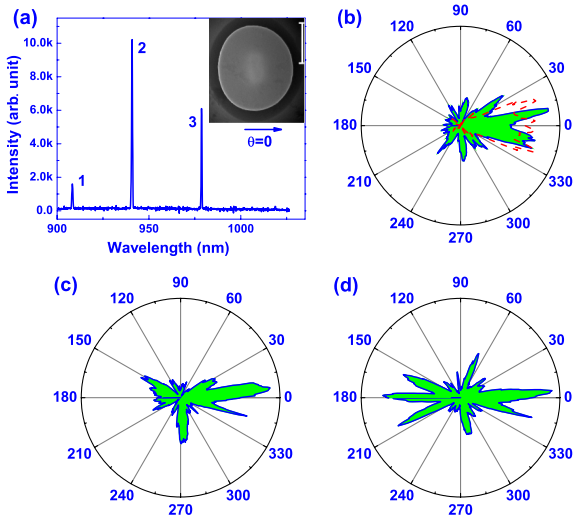

FIG. 1 (color online). (a) Inset: Top-view SEM image of a GaAs disk. The scale bar is 1 μm. Main panel: Measured laser emission spectrum at the incident pump intensity of 191 W/cm^2. (b)–(d) Measured FFPs for the lasing modes 1, 2, and 3 shown in (a). The red dashed curve in (b) is the FFP obtained by a ray-tracing model [4] applied to the cavity in the inset of (a).

The lasing characteristic, e.g., the threshold behavior of emission intensity versus pumping level and the dramatic narrowing of spectral peaks, is similar to that of larger disks which was reported in Ref. [12]. Because we are measuring the lasing spectrum, only the HQM of frequencies within the gain spectrum are accessible. Since the gain spectrum of InAs quantum dots is inhomogeneously broadened and has a large width of ~80 nm, we are able to observe several lasing modes in the small disk despite the large mode spacing. The laser emission spectrum [Fig. 1(a)] consists of three peaks at vacuum wavelengths $\lambda = 908$, 942, and 978 nm. The far-field patterns (FFPs) of these three modes are dramatically different [Figs. 1(b)–1(d)]. The lasing mode at 908 nm has output mostly in forward direction ($\theta_{\mathrm{FF}} = 0°$), while the 978 nm mode has bidirectional emission in forward and backward ($\theta_{\mathrm{FF}} = 180°$) directions, and the 942 nm mode is intermediate between the two patterns. This phenomenon is fundamentally different from that of larger disks, in which all lasing modes produce emission in forward direction.

The origin of universal directional emission in larger ARCs is the following. As long as the phase space is sufficiently chaotic, i.e., the deformation is large enough, there is the possibility of chaotic motion (diffusion) in phase space from the totally internally reflected region defined by $|\sin\chi| > 1/n$ (χ is the incident angle and n the effective index of the cavity) until refractive ray escape is allowed [4]. Because of interference effects such as dynamical localization (in phase space) and scarring (localization of eigenstates along the UPOs), the center of the electromagnetic (EM) wave function may be localized above the critical angle, leading to high Q, but its tail which dominates the escape follows the unstable manifolds associated with short UPOs [5,10,11]. The shape-specific emission pattern is calculated by a model which combines phase space ray tracing with a modified version of TE or TM Fresnel scattering for escape; performing such calculations for the TE case appropriate for our cavity gives the results shown in Fig. 1(b) (dashed line). Consistent with other calculations for similar shapes [11], we find broad but unidirectional emission in forward direction.

The failure of the ray model in wavelength-scale ARC lasers is expected; this statistical model is more appropriate for multimode lasing in the limit of short wavelength ($kR \gg 1$, $k = 2\pi/\lambda$). However the persistence of unidirectional emission to such small scales is surprising. As $kR \to 1$, the mode spacing becomes larger and the deformation of the shape from circular symmetry is effectively a weaker perturbation. Thus one would expect HQMs to appear as smooth deformations of conventional whispering gallery (WG) modes of the circle, with large angular momentum and roughly isotropic emission. The LQMs with small angular momentum will be more anisotropic, but these modes would not show up in the lasing spectrum because their lasing thresholds are too high. To see why this expectation is violated in the experiment, we calculated the lasing spectrum for the actual cavity shape, extracted from SEM images. Since the system is inhomogeneously broadened and relatively high Q, modal interactions are negligible so the lasing modes are essentially the same as passive cavity resonances (we confirmed this by comparison with nonlinear calculations [13]). Three numerical methods were used to find the cavity resonances [12,14,15]; they give consistent results. We find a set of HQMs with constant frequency spacing and similar spatial profile; in most cases these modes do indeed look like WG modes, with vanishing intensity towards the disk center. However, as shown in Fig. 2, their Q values have an unusual nonmonotonic variation with frequency, exhibiting a minimum at $kR \sim 7.1$. In addition, we find a LQM series in the same frequency range, the relevance of which will be discussed below.

To characterize the directionality of the output we define $U \equiv \int I(\theta_{\mathrm{FF}})\cos\theta_{\mathrm{FF}} d\theta_{\mathrm{FF}} / \int I(\theta_{\mathrm{FF}}) d\theta_{\mathrm{FF}}$, where $I(\theta_{\mathrm{FF}})$ represents the angular distribution of FFP; $U = 0$ corresponds to isotropic or bidirectional emission, whereas positive (negative) U corresponds to emission primarily in forward (backward) direction. We find that as kR decreases from 10 to 5.5, the value of U in the HQM series first increases from approximately 0 to 0.6 and then decreases to 0 [Fig. 2(b)]. The calculated FFPs confirm a transition from bidirectional emission to unidirectional emission, and back to bidirectional emission. The kR value at which U is maximal is close to but not equal to that of the mode with the minimum Q for the HQM series. Our lasing experiment, however, cannot detect the lowest Q mode of the series [labeled 4 in Fig. 2(a)] because it does not lase; instead the three modes it measures [Fig. 1(a)] are the ones on the low kR (long wavelength) side of the Q dip [labeled 1, 2, and 3 in Fig. 2(a)]. The calculated FFPs are in good agreement with the measured ones, which are also plotted in Fig. 2(b).

The dip in Q of the HQM series is associated with the unidirectional emission; we therefore analyze the highest and lowest Q modes (1 and 4 in Fig. 2) on the long wavelength side for a clue to the mechanism of the unidirectional emission. The intensity plots for these two modes in Figs. 3(a) and 3(d) show that while mode 1 is a smooth

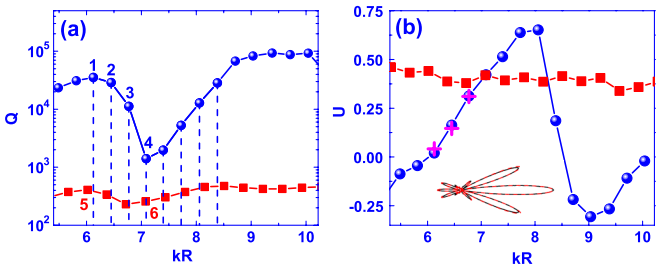

FIG. 2 (color online). (a) Calculated Q values for the HQMs (blue dots) and the LQMs (red squares) in the same cavity as that in Fig. 1. Modes marked 1, 2, and 3 correspond to the three lasing modes in Fig. 1. (b) Calculated values of directionality U for the HQMs and LQMs versus kR. Crosses are U values of three lasing modes in Fig. 1. Inset: Calculated FFPs for modes labeled 4 (black solid line) and 6 (red dashed line) in (a).

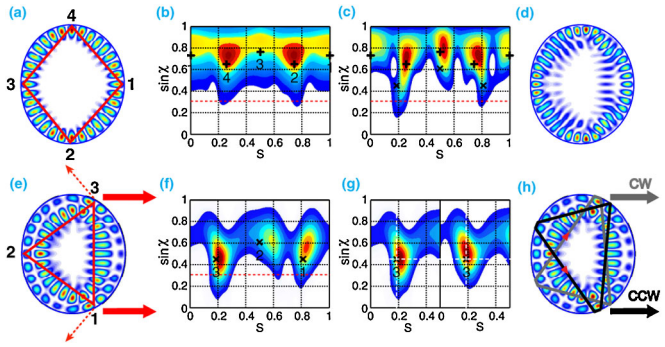

FIG. 3 (color online). (a),(d),(e) Calculated magnetic field intensity for the TE cavity modes labeled 1, 4, 5 in Fig. 2(a); red arrows in (e) indicate high emission directions based on chiral symmetry; however, the dashed arrows denote emission which is not observed in the experiment (see below). Panels (b), (c),(f) show their Husimi projections (incident) onto the Poincaré SOS. The horizontal axis S is the arc length along the cavity boundary from the point $\theta = 0$ normalized by the cavity perimeter, the vertical axis is $\sin\chi$. The red dashed lines mark the critical angle for total internal reflection. The bouncing points of a diamond orbit (or triangle orbit), drawn in (a) or (e), are marked by "+" (or "×") and labeled in (a) and (b) or (e) and (f). Panel (g) compares the incident and emergent Husimi projections of mode 5 for CW waves; the shift of the emergent waves to smaller S and higher $\sin\chi$ directly demonstrates the GHS and FF effects in our device. (h) Two distinct periodic pseudo-orbits (gray and black) for CW and CCW waves which give rise to unidirectional emission instead of the tridirectional emission expected from the periodic triangle ray orbit shown in (e).

deformation of a WG mode with angular momentum $m = 16$, mode 4 appears to be a mixture of a similar WG mode and a much lower angular momentum mode with significant intensity away from the boundary.

Any EM "wave function" can be given a classical (ray) interpretation via the Husimi function which is a smoothed version of the Wigner transform. In a leaky quantum billiard, the most useful representation is to project the Husimi distribution onto the classical surface of section (SOS) [14,16]. The SOS displays phase space trajectories as points in a 2D plot with coordinates S and $\sin\chi$. The Husimi projection gives the precise "ray content" of the mode at the boundary in terms of a density of rays and their angle of incidence. The Husimi maps for our cavities indicate more clearly than the real-space intensities that the modes of interest are structured around short UPOs. For mode 1 the incident Husimi function [in Fig. 3(b)] has four maxima at points on the boundary and angles of incidence fairly close to those of the "diamond orbit," which is superposed on the wave function in Fig. 3(a). The Husimi density below the critical angle has the largest amplitude near the bounce points labeled 2 and 4 ($S = 0.26$ and 0.73), which are the points of highest curvature among the four bounce points; most of the emission occurs there. Note that the Husimi map for this mode in Fig. 3(b) has approximate reflection symmetry about the vertical lines passing the points $S = 0, 0.5$, leading to approximately equal emission into the forward and backward quadrants. In contrast, the Husimi function for mode 4 [Fig. 3(c)] shows a large symmetry breaking around $S = 0.5$, which leads to the unidirectional emission primarily from the region around $S = 0.2$ on the boundary in forward direction. Note that we display only the upper half ($\sin\chi > 0$) portion of the SOS corresponding to clockwise (CW) circulating rays; the Husimi function in the lower half is reflected around $S = 0.5$ and indicates strong emission from $S = 0.8$ but of the oppositely circulating [counterclockwise (CCW)] ray, leading to far-field emission in forward direction as well.

The reason mode 4 has lower Q and more directional emission than mode 1 lies in its coupling [17] to the LQM also shown in Fig. 2. A typical mode in the LQM series, e.g., mode 5 in Figs. 3(e) and 3(f), has a Husimi function well localized near a three-bounce orbit. Since this orbit has two bounce points (labeled 1 and 3) much closer to the critical angle, this mode series has much lower Q than the series based on the diamond orbit and does not lase experimentally. This is consistent with our expectation that the more directional modes would not appear in the lasing spectrum.

However, the two HQM and LQM series have different frequency spacing, and thus it is possible to have particular pairs of modes (one from each series) which are nearly degenerate in the real part of their frequencies. This is exactly what happens for the modes labeled 4 and 6 in Fig. 2, and the resultant mixing of the two modes leads to the dip in the Q of mode 4 and its strong directionality of emission. In Figs. 3(c) and 3(d) one clearly sees that mode 4 is a mixture of modes 1 and 5; this is the case for mode 6 as well (not shown), which has "more" of the leakier mode 5 and hence lower Q. As shown in the inset of Fig. 2(b), the FFPs for modes 4 and 6 are nearly identical, confirming they are coupled and the output is dominated by the LQM component.

Thus an isotropic HQM can become a directional emitter by means of weak coupling to a directional LQM which does not strongly degrade the Q, but enables substantially directional output. In general, when two complex resonance frequencies approach one another, two scenarios are possible: weak coupling in which the frequencies cross and the Q values anticross (no "exchange of identity") or strong coupling in which the frequencies anticross and the Q values cross ("exchange of identity") [18]. We have verified numerically that in the current experiment the weak coupling scenario is realized by changing the cavity shape through a slow variation of ϵ_1 and directly observing the crossing of frequencies and anticrossing of Q values [19]. While mode 4 is the most hybridized (and therefore too low Q to lase), the mode coupling for the experimentally observed mode 3 is sufficient to obtain directional emission. Its Q exceeds 10 000, high enough to lase with modest pumping.

A final intriguing question is how to explain the broken symmetry of emission of the LQM series based on the

triangle orbit. The orbit itself has symmetric bounce points [labeled 1 and 3 in Fig. 3(e)] which are at lower incidence angle than bounce 2, and hence are the points where most of the emission should occur. A ray can traverse the triangle either CW or CCW, and because of this symmetry "triangle modes" should emit at each point into the forward *and* backwards quadrants [see Fig. 3(e)]. If this chiral symmetry between CW and CCW propagation were obeyed by the EM wave function, the unidirectionality would be lost, but the Husimi map of Fig. 3(f) describing CW rays ($\sin\chi > 0$) violates this symmetry and is indeed leakier at point 3 than point 1. The Husimi map for CCW rays ($\sin\chi < 0$) has the opposite asymmetry and is leakier at point 1, leading to the unidirectional emission.

This symmetry breaking can only come from the openness of the system. A qualitative explanation is based on two effects of the openness of the cavity which become more important at the wavelength scale. One is "Fresnel filtering" (FF), a correction to the specular reflection and Snell's law of refraction of beams at a dielectric interface, due to their spread in transverse momentum [20,21]. It has the effect of deflecting the reflected beam away from the normal. The other is the "Goos-Hänchen" shift (GHS) [22], a lateral displacement (of order the wavelength) of a beam totally internally reflected from a flat dielectric interface. The CW and CCW components in ARCs behave essentially like trapped beams and "violate" ray dynamics due to these two effects. One can capture this effect semiquantitatively with a modified ray dynamics in which the incident ray is translated along the boundary in the direction of motion according to the GHS law, before emerging at an angle of reflection greater than its angle of incidence due to the FF effect. This modified ray dynamics violates the chiral symmetry of the periodic orbits; a periodic orbit such as the triangle will now break into two distinct CW and CCW periodic pseudo-orbits [21]. Here we point out that this chiral symmetry breaking is essential to obtain unidirectional emission in our system. The modified ray dynamics of Ref. [21] is only an approximation because it neglects the curvature of the boundary, so we have here inferred the actual CW and CCW pseudo-orbits of our resonator from analysis of the emergent and incident Husimi distributions [see Fig. 3(g)]. The results are shown in Fig. 3(h): the CW orbit has a much smaller angle of incidence near bounce point 3 than does the CCW orbit, leading to unidirectional forward emission dominated by the CW beam; the corresponding effect occurs for the CCW orbit near bounce point 1, so it dominates the emission, again in forward direction. Note that both orbits show a GHS which varies approximately as expected, reaching a maximum at the critical angle.

In conclusion, we have demonstrated directional output from an ARC laser of dimensions comparable to the emission wavelength. The unidirectional emission is based on weak coupling of isotropic HQMs to directional LQMs and chiral symmetry breaking due to violations of ray optics on the wavelength scale. Numerical simulations indicate that similar behavior occurs for a wide range of cavity deformations around that studied here ($0.3 \leq \epsilon \leq 0.49$, $0 \leq \epsilon_1 \leq 0.1$) and indices of refraction ($n = 2.4$–3.9), making our design potentially useful for GaN lasers at blue and near-UV wavelengths as well.

This work is supported partly by NIST under Grant No. 70NANB6H6162, by NSF under Grants No. DMR-0808937 and No. DMR-0908437, and by the DFG research group 760.

[1] *Optical Microcavities*, edited by K. J. Vahala, Advanced Series in Applied Physics (World Scientific, Singapore, 2004).
[2] Z. Y. Zhang *et al.*, Appl. Phys. Lett. **90**, 111119 (2007).
[3] Q. H. Song *et al.*, Appl. Phys. Lett. **94**, 061109 (2009).
[4] J. U. Nöckel and A. D. Stone, Nature (London) **385**, 45 (1997).
[5] H. G. L. Schwefel *et al.*, J. Opt. Soc. Am. B **21**, 923 (2004).
[6] C. Gmachl *et al.*, Science **280**, 1556 (1998).
[7] T. Harayama *et al.*, Phys. Rev. Lett. **91**, 073903 (2003).
[8] Y. Baryshnikov *et al.*, Phys. Rev. Lett. **93**, 133902 (2004).
[9] M. Lebental *et al.*, Appl. Phys. Lett. **88**, 031108 (2006).
[10] S.-B. Lee *et al.*, Phys. Rev. A **75**, 011802(R) (2007).
[11] J. Wiersig and M. Hentschel, Phys. Rev. Lett. **100**, 033901 (2008).
[12] Q. H. Song *et al.*, Phys. Rev. A **80**, 041807(R) (2009); S. Shinohara *et al.*, *ibid.* **80**, 031801(R) (2009); C. L. Yan *et al.*, Appl. Phys. Lett. **94**, 251101 (2009); C. H. Yi *et al.*, *ibid.* **95**, 141107 (2009).
[13] H. E. Tureci *et al.*, Science **320**, 643 (2008).
[14] H. E. Tureci *et al.*, *Progress in Optics*, edited by E. Wolf (Elsevier, New York, 2005), Vol. 47, Chap. 2.
[15] J. Wiersig, J. Opt. A **5**, 53 (2003).
[16] M. Hentschel, H. Schomerus, and R. Schubert, Europhys. Lett. **62**, 636 (2003).
[17] The coupling here is the linear coupling of two eigenvalues near a frequency crossing, not the nonlinear coupling of modes due to spectral hole burning, which is negligible in our device due to the inhomogeneous gain broadening.
[18] J. Wiersig and M. Hentschel, Phys. Rev. A **73**, 031802 (2006).
[19] See supplementary material at http://link.aps.org/supplemental/10.1103/PhysRevLett.105.103902 for the proof of weak coupling between HQM and LQM.
[20] H. E. Tureci and A. D. Stone, Opt. Lett. **27**, 7 (2002).
[21] E. G. Altmann, G. Del Magno, and M. Hentschel, Europhys. Lett. **84**, 10 008 (2008).
[22] J. Unterhinninghofen, J. Wiersig, and M. Hentschel, Phys. Rev. E **78**, 016201 (2008).